

---

# Learning Depthwise Graph Convolution from Data Manifold

---

**Guokun Lai**

Language Technologies Institute  
Carnegie Mellon University  
guokun@cs.cmu.edu

**Hanxiao Liu**

Language Technologies Institute  
Carnegie Mellon University  
hanxiaol@cs.cmu.edu

**Yiming Yang**

Language Technologies Institute  
Carnegie Mellon University  
yiming@cs.cmu.edu

## Abstract

Convolution Neural Network (CNN) has gained tremendous success in computer vision tasks with its outstanding ability to capture the local latent features. Recently, there has been an increasing interest in extending convolution operations to the non-Euclidean geometry. Although various types of convolution operations have been proposed for graphs or manifolds, their connections with traditional convolution over grid-structured data are not well-understood. In this paper, we show that depthwise separable convolution can be successfully generalized for the unification of both graph-based and grid-based convolution methods. Based on this insight we propose a novel Depthwise Separable Graph Convolution (DSGC) approach which is compatible with the tradition convolution network and subsumes existing convolution methods as special cases. It is equipped with the combined strengths in model expressiveness, compatibility (relatively small number of parameters), modularity and computational efficiency in training. Extensive experiments show the outstanding performance of DSGC in comparison with strong baselines on multi-domain benchmark datasets.

## 1 Introduction

Convolution Neural Network (CNN) (LeCun et al., 1995), also referred to as 2D-convolution in the following paper, has been proven to be an efficient model family in extracting hierarchical local patterns from grid-structured data, which has significantly advanced the state-of-the-art performance of a wide range of machine learning tasks, including image classification, object detection and audio recognition (LeCun et al., 2015). Recently, growing attention has been paid to dealing with data with a non-grid structure, such as prediction tasks in sensor networks (Xingjian et al., 2015), transportation systems (Li et al., 2017), and 3D shape correspondence application in the computation graphics (Bronstein et al., 2017). How to replicate the success of CNNs for manifold-structured data remains an open challenge.

In this paper, we provide a unified view of the 2D-convolution methods and the graph convolution (including the geometric convolution) with the label propagation process (Zhu et al., 2003). To best of our knowledge, it is the first time that the 2D-convolution and graph convolution proposed in (Kipf and Welling, 2016) are unified mathematically. It helps us better understand and compare the difference between them, and shows that the fundamental difference can be summarized as two

points, (1) 2D-convolution learns spatial filters from the data. (2) Spatial filters in 2D-convolution are channel-specific.

Many graph convolution and geometric convolution methods have been proposed recently. The spectral convolution methods (Bruna et al., 2013; Defferrard et al., 2016; Kipf and Welling, 2016) are the mainstream algorithms developed as the graph convolution methods. Their theory is based on the graph Fourier analysis (Shuman et al., 2013). Another group of approaches are geometric convolution methods, which focus on various ways to leverage spatial information about nodes (Masci et al., 2015; Boscaini et al., 2016; Monti et al., 2016; Gilmer et al., 2017). Existing models mentioned above are either fully trusting the given graph or applying one graph filter across all channels, which are corresponding to the two differences between the traditional 2D-convolution and the graph convolution. Firstly, as a result of trusting the given graph, namely only using a given graph filter across the whole model, the model ability to discover the special graph filters from the supervision data is limited. And applying one graph filter across all channels would also introduce several drawbacks to the model as follows. (1) It makes the mathematical formulation of the graph convolution methods incompatible with the traditional 2D-convolution. (2) The model cannot propagate information with different diffusion patterns in one layer. (3) The image recognition experiment in Section 5.2 shows that multiple filters are critical to the model performance in the task which requires extracting complex local features. Some models, such as MoNet (Monti et al., 2016) and Graph Attention Network (Veličković et al., 2017), try to model multiple filters by simultaneously learning  $K$  sub-layers, each with one global filter, and summarizes them as one layer. However, this approach would lead to a larger number of parameters and more expensive computation cost, and it is still incompatible with the traditional 2D-convolution method.

In this paper, we derive a novel graph convolution approach directly from the 2D-convolution method. We propose the Depthwise Separable Graph Convolution (DSGC), which inherits the strength of depthwise separable convolution that has been extensively used in different state-of-the-art image classification frameworks including Inception Network (Szegedy et al., 2016), Xception Network (Chollet, 2016) and MobileNet (Howard et al., 2017). Compared with previous graph and geometric methods, the DSGC is more expressive and compatible with the depthwise separable convolution network, and shares the desirable characteristic of small parameter size as in the depthwise separable convolution. In experiments section, we evaluate the DSGC and baselines in three different machine learning tasks. The experiment results show that the performance of the proposed method is close to the standard convolution network in the image classification task on CIFAR dataset. And it outperforms previous graph convolution and geometric convolution methods in all tasks. Furthermore, we demonstrate that the proposed method can easily leverage the state-of-the-art architectures developed for image classification to enhance the model performance, such as the Inception module (Szegedy et al., 2016), the dense block (Huang et al., 2016) and the Squeeze-and-Excitation block (Hu et al., 2017).

The main contribution of this paper is threefold:

- A unified view of traditional 2D-convolution and graph convolution methods by introducing depthwise separable convolution.
- A novel Depthwise Separable Graph Convolution (DSGC) for data residing on arbitrary manifolds.
- We demonstrate the efficiency of the DSGC module with extensive experiments and show that it can be plugged into existing state-of-the-art CNN architectures to improve the performance for graph tasks.

## 2 A Graph Perspective of Convolution

In this section, we provide a unified view of several convolution operations by showing that they are different message aggregation protocols over the graphs or manifolds. Unless otherwise specified, we denote a matrix by  $\mathbf{X}$ , the  $i$ -th row in the matrix by  $x_i$ , and the  $(i, j)$ -th element in the matrix by  $x_{ij}$ . Superscripts are used to distinguish different matrices when necessary. All the operations below can be viewed as a function that transforms input feature maps  $\mathbf{X} \in \mathbb{R}^{N \times P}$  to output feature maps  $\mathbf{Y} \in \mathbb{R}^{N \times Q}$ , where  $N$  is the number of nodes and  $P, Q$  are the number of its associated input and output features (channels) respectively. We use  $\mathbf{G}$  to denote the adjacency matrix of a graph, and

$G(i)$  to denote the set of neighbors for node  $i$ . For tasks over sensor networks (Xingjian et al., 2015), transportation graphs (Li et al., 2017) or computational graphics (Bronstein et al., 2017), graph  $G$  often corresponds to the latent structure of the underlying manifold, and is induced from the spatial coordinates of input data.

## 2.1 Convolution over Graphs

For the operations discussed below, the filter weights are fully determined by the given graph  $G$ .

### 2.1.1 Label Propagation

Label propagation (LP) (Zhu et al., 2003) can be viewed as a simplistic convolution operation to aggregate local information over a graph:

$$\mathbf{y}_i = \sum_{j \in G(i)} G_{ij} \mathbf{x}_j \quad (1)$$

In other words, the feature map for each node is updated as the weighted combination of its neighbors' feature maps. In this case, the numbers of input and output channels are identical.

### 2.1.2 Graph Convolution

Graph convolution (Kipf and Welling, 2016) (GC) can be viewed as an extension of LP, formulated as:

$$\mathbf{y}_i = \sum_{j \in G(i)} G_{ij} \mathbf{z}_j \quad \text{where} \quad \mathbf{z}_j = \mathbf{x}_j \mathbf{U} \quad (2)$$

While both LP and GC utilize the graph structure in  $G$ , GC has an learnable linear transformation  $\mathbf{U} \in \mathbb{R}^{P \times Q}$  that maps  $\mathbf{x}_j$  into the intermediate representation  $\mathbf{z}_j$ . This additional step enables GC to capture the dependencies among channels.

## 2.2 Convolution over Grid-Structures

Here, we write the convolution methods over 2D-grid in the Label Propagation framework. Let  $\Delta_{ij}$  be the coordinate offset from  $i$ -th node to  $j$ -th node, we say  $j \in G(i)$  if  $j$  is one of  $i$ 's  $k$ -nearest neighbors based on the relative distance  $|\Delta_{ij}|$ .

### 2.2.1 Full Convolution

The full convolution (LeCun et al., 1995) can be formulated as

$$y_{iq} = \sum_{j \in G(i)} \sum_{p=1}^P w_{\Delta_{ij}}^{(pq)} x_{jp} \quad (3)$$

For Euclidean grid-structured data such as images,  $\Delta_{ij}$  denotes the offset between pixel  $i$  and pixel  $j$ , and  $G(i)$  contains pixel  $i$ 's surrounding pixels. For example, the size of  $G(i)$ , or  $k$ , is 9 for  $3 \times 3$  convolution and 25 for  $5 \times 5$  convolution, corresponding to the size of the receptive field. The full convolution operation captures the channel correlation and spatial correlation simultaneously by  $\mathbf{W}^{(pq)}$ .

### 2.2.2 Depthwise Separable Convolution

The Depthwise Separable Convolution (DSC) (Chollet, 2016) is a factorized version of full convolution under the intuition that the channel correlation and spatial correlation can be decoupled. In practice, DSC is able to achieve comparable performance as full convolution with a substantially smaller number of parameters. We focus on DSC here due to its simplicity and intimate connections to Graph Convolution. DSC can be formulated in a graph-based fashion as follows

$$y_{iq} = \sum_{j \in G(i)} w_{\Delta_{ij}}^{(q)} z_{jq} \quad \text{where} \quad \mathbf{z}_j = \mathbf{x}_j \mathbf{U} \quad (4)$$

The formulation of DSC is analogous to GC by substituting  $G$  in eq. (2) with  $W$ . However, unlike LP and GC which directly utilize the graph  $G$  to define their filter weights, weights  $W$  in eq. (4) is a learnable lookup table of size  $Q \times R$ , where  $R$  is the number of possible choices for  $\Delta_{ij}$ . For example,  $R = 9$  for  $3 \times 3$  convolution, since  $\Delta_{ij}$  can take any value in  $\{-1, 0, 1\} \times \{-1, 0, 1\}$ .

### 3 Depthwise Separable Graph Convolution

#### 3.1 Motivation

We notice that DSC is more powerful than GC in the following aspects:

1. The spatial filter in GC is fully determined once the graph is given<sup>1</sup>, but the spatial filters in DSC are learned automatically from data. This means GC would fully trust the given graph even if it is suboptimal for the task and data on hand.
2. Compared with full convolution and DSC, which are capable of modeling channel-specific convolution filters, GC uses a global spatial filter for all channels (features), which can be viewed as a restricted version of DSC. Thus a GC module is unable to simultaneously capture or fuse diverse information based on different channels/features over the graph.

On the other hand, while GC is generally applicable to arbitrary graphs, the DSC method so far is only designed for regular grid-based structures and hence only applicable to the domains like image processing, where the pixels naturally form a grid structure. For nodes scattered with arbitrarily spatial coordinates, the number of possible choices for  $\Delta_{ij}$  can be infinite. That is, using a lookup table  $W$  to memorize the filter weights for each  $\Delta_{ij}$  is no longer feasible. This makes traditional DSC not directly applicable to arbitrary graphs.

#### 3.2 Proposed Method

To address the aforementioned limitations of Graph Convolution, we propose Depthwise Separable Graph Convolution (DSGC), which naturally generalizes DSC and GC as:

$$y_{iq} = \sum_{j \in G(i)} w^{(q)}(\Delta_{ij}) z_{jq} \quad \text{where} \quad z_j = x_j U \quad (5)$$

where we slightly abuse the notation by overloading  $w^{(q)}(\cdot)$  as a function (neural network) that maps  $\Delta_{ij}$  to a real scalar, namely the predicted filter weight for the  $q$ -th channel.

The key distinctions in our formulation are as follows.

1. Different from DSC (eq. (4)), the filter weight is calculated using a “soft” function approximator. That is, DSGC predicts the convolution filter weights from  $\Delta_{ij}$  via the function instead of memorizing them in a look-up table. In our experiments, function  $w^{(q)}(\cdot)$  is implemented as a two-layer MLP.
2. Different from GC (eq. (2)), DSGC enables the learning of channel-specific spatial convolution filters (channels are indexed by  $q$  in eq. (5)). This amounts to simultaneously constructing channel-specific graphs under the different node-node similarity metrics, where the metrics are implicitly defined by neural networks and hence, are jointly optimized during the training.

The idea of predicting the filter weights has also been explored in Message Passing Neural Network (MPNN) (Gilmer et al., 2017). However, MPNN learns only a global function across all channels, hence, MPNN is incapable of capturing channel-specific spatial filters as in DSC.

#### 3.3 Parameter Grouping Strategy

Overfitting is a common issue in graph-based applications due to limited data available. To alleviate this issue, a simple strategy is to group the original  $Q$  channels into  $C$  groups, where  $D = Q/C$

<sup>1</sup>The linear transformation  $U$  in GC is not a graph/spatial filter, as it only fuses the information across the channels.

channels in the same group would share the same filter:

$$w^{(q)}(\cdot) = w^{(q')}(\cdot) \quad \text{if} \quad \lfloor \frac{q}{D} \rfloor = \lfloor \frac{q'}{D} \rfloor \quad (6)$$

where  $\lfloor \cdot \rfloor$  denotes the floor function.

### 3.4 Filter Normalization

A common practice in label propagation and graph convolution is to normalize the adjacency matrix for  $G$ . In DSGC, a natural way to carry out normalization is to apply a softmax function as the final layer of the filter weights predictor, to ensure that  $\sum_{j \in G(i)} w^{(q)}(\Delta_{ij}) = 1$  for each  $i$ . We empirically found that normalization leads to improved performance and faster convergence.

## 4 Closely Related Models

Several representative works in graph convolution are worth discussing w.r.t. their connections to ours.

### 4.1 Spectral Convolution Methods

The Spectral Network (Bruna et al., 2013) is derived from the graph signal processing work (Shuman et al., 2013), which generalizes Fourier analysis for its use in the graph domain as:

$$y_{iq} = \sum_{j \in G(i)} \sum_{p=1}^P w_{ij}^{(pq)} x_{jp} \quad (7)$$

where  $\mathbf{W}^{(pq)} = \Phi \Lambda^{(pq)} \Phi^T$

where  $\Phi \in \mathbb{R}^{n \times n}$  are the eigenvectors of  $G$ 's graph Laplacian matrix, and  $\Lambda$  are learnable nonparametric filters from the training data. The Spectral Network can be matched with the full convolution (eq.(3)), but with the different filter subspace, in other words, with different basic filters. Limitations of Spectral Networks include its high computation cost due to eigen-decomposition of the graph Laplacian, the lack of spatial locality and the large number of parameters which grows linearly over the graph size.

These limitations are partially addressed in the Chebyshev Networks (Defferrard et al., 2016) (ChebyNet), which approximates the non-parametric filters as:

$$y_{iq} = \sum_{j \in G(i)} \sum_{k=1}^K T_k(L)_{ij} z_{jq}^{(k)}, \quad \mathbf{z}_j^{(k)} = \mathbf{x}_j \mathbf{U}^{(k)} \quad (8)$$

where  $T_k(L)$  is the  $k$ -th order Chebyshev polynomial term. While being faster than Spectral Networks, ChebyNet suffers from insufficient expressiveness, similar to the limitations of GC. The expressiveness of ChebyNet can be improved by enlarging  $K$ , which requires a much larger number of parameters and eventually converges to Spectral Networks.

### 4.2 Geometric Convolution Methods

Several geometric convolution methods (Masci et al., 2015; Boscaini et al., 2016; Monti et al., 2016) are proposed for manifold structured data, among which MoNet (Monti et al., 2016) is the state-of-the-art.

The updating formula for MoNet can be written as

$$y_{iq} = \sum_{j \in G(i)} \sum_{k=1}^K w_k(v(i, j)) z_{jq}^{(k)}, \quad \mathbf{z}_j^{(k)} = \mathbf{x}_j \mathbf{U}^{(k)} \quad (9)$$

$$w_k(v) = \exp\left(-\frac{1}{2}(v - \mu_k)^T \Sigma_k^{-1} (v - \mu_k)\right)$$

where  $v(i, j)$  is the embedding of a node pair similar to  $\Delta_{ij}$  in our model, and  $\mu_k, \Sigma_k$  are both learnable parameters. MoNet can be viewed as an extension of ChebyNet where the graph filters are learned from data instead of being fully determined by a given graph. However, a graph filter in MoNet is still applied across all channels. In order to have  $k$  filters in MoNet, it needs to learn  $k$  different channel filters  $U$ . Then the total number of model parameters will grow linearly with  $k$ . While DSGC only learns a channel filter  $U$  for one layer. By taking advantage of that, the number of parameters in DSGC would not be significantly growing with  $k$  as MoNet. Similar to it, the recently proposed Graph Attention Network (GAT) (Veličković et al., 2017) is also required to learn multiple channel filters in order to model multiple filters in one layer, which would lead to a larger number of the model parameters. Furthermore, in the setting that nodes in graph have geometric information, GAT can be viewed as a MoNet extension with the filter normalization trick. We empirically found that the extension exhibits obvious improvement over the original MoNet. In the following parts, we denote it as MoNet with GAT.

Message Passing Neural Networks (MPNN) (Gilmer et al., 2017; Schütt et al., 2017) are developed for modeling information propagation over graphs, specialized for the prediction tasks in quantum chemistry. Similar to DSGC, MPNN utilizes a neural network to predict the filter weights for the convolution operations. The key difference is that while DSGC allows channel-specific graph convolution filters (hence allowing a variety of diffusion patterns over the graph), MPNN learns only a single graph filter function for all channels in a layer. So MPNN can be viewed as a special case of DSGC with  $C = 1$  in eq. (6). In our experiments, our method consistently outperforms MPNN across tasks in a variety of domains.

## 5 Experiments

### 5.1 Experimental Design

Our experiments for evaluating the proposed DSGC approach consists of three parts. Firstly, we evaluate DSGC on a popular image classification dataset (Sec. 5.2). The purpose is to confirm the strong performance of DSGC in handling grid-based convolution although it is designed for more general graph structures. Secondly, we compare DSGC and strong methods in the tasks of time series forecasting (Sec. 5.3) and text categorization (Sec. 5.4) where grid-based convolutions are invalid but graph convolution would have advantages instead as they are designed for more flexible graph structures. Thirdly, we examine the flexibility and effectiveness of using DSGC as a building block (module) in multiple well-known neural network architectures, including Inception (Szegedy et al., 2016), DenseNet framework (Huang et al., 2016) and etc. (See Appendix A.1).

For controlled experiments, all the graph convolution methods share the same empirical settings unless otherwise specified, including network structures, the dimension of latent factors, and hyper-parameter tuning process. The neural network used to model the spatial convolution filter ( $w^{(q)}(\cdot)$ ) in eq. (5) is a two-layer MLP with 256 hidden dimensions and tanh activation function. We have conducted ablation tests with the two-layer MLP by changing the number of layers and activation function of each hidden layer, and by trying several weight sharing strategies. The results are very similar; the two-layer MLP provides a reasonable performance with the shortest running time. Appendix B contains more details, such as the network architecture and model hyper-parameters. The algorithms are implemented in PyTorch; all the data and the code including baselines are made publicly accessible <sup>2</sup>.

### 5.2 Evaluation on Image Classification

We conduct experiments on CIFAR10 and CIFAR100 (Krizhevsky and Hinton, 2009), which are popular benchmark datasets in image classification. Both sets contain 60000 images with  $32 \times 32$  pixels but CIFAR10 has 10 category labels and CIFAR100 has 100 category labels. Each image is typically treated as a  $32 \times 32$  grid structure for standard image-based convolution. To enable the comparison on generic graphs, we create the modified versions of CIFAR10 and CIFAR100 respectively, by subsampling only 25% of the pixels from each graph. As illustrated in Figure 1, the subsampling result is irregularly scattered nodes for each image. The detailed experiment settings are included in Appendix B.1.

<sup>2</sup>Code and Data: the links are anonymous due to the double-blind policy.

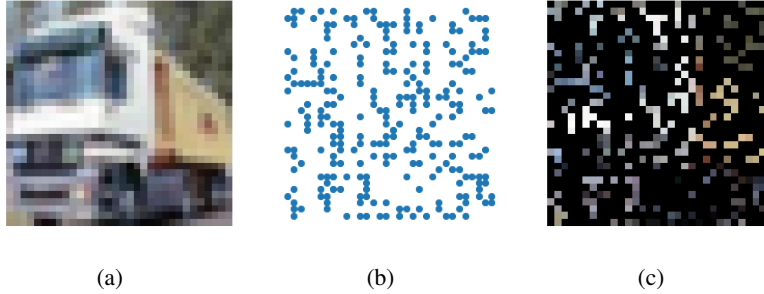


Figure 1: How to construct subsampled CIFAR datasets: (a) is an example image from CIFAR dataset. (b) is the subsampled pixels map. The blue points indicate which points are sampled. (c) is the image after sampling, where the black points are those not being sampled.

For all methods, we use the VGG-13 architecture (Simonyan and Zisserman, 2014) as the basic framework, and replace its convolution layers with different convolution modules. The experiment results are summarized in Table 1. The best performances among the graph-based neural networks are in bold. Firstly, we observe that Xception and CNN have the best results; this is not surprising because both methods use grid-based convolution which is naturally suitable for image recognition. Secondly, DSGC outperforms all the other graph-based convolution methods, and its performance is very close to that of the grid-based convolution methods. We also see that the models that learn multiple filters (DSGC and MoNet) have better performance than the models that only learn one global graph filter, such as MPNN and GCN. It demonstrates that it is necessary to enable multiple filters in this task. Furthermore, contributed by the depthwise separable convolution and graph sharing technique, our model can achieve a competitive performance without increasing the number of parameters as GCN, the one with the smallest number of parameters among graph convolution approaches. On the contrary, MoNet and ChebyNet have a relatively larger number of parameters in order to model multiple filters in one layer. In Appendix A.2, we analyze the computation cost and training time of the proposed DSGC and baseline methods.

Method	Subsampled Images			Original Images		
	CIFAR10	CIFAR100	#params	CIFAR10	CIFAR100	#params
DCNN (Atwood and Towsley, 2016)	43.68%	76.65%	12M	55.56%	84.16%	50M
ChebyNet (Defferrard et al., 2016)	25.04%	49.44%	10M	12.99%	36.96%	19M
GCN (Kipf and Welling, 2016)	26.78%	51.30%	5.6M	19.09%	41.64%	9.8M
MoNet (with GAT) (Monti et al., 2016)	21.20%	47.87%	11M	8.34%	29.56%	20M
MPNN (Gilmer et al., 2017)	22.71%	49.03%	5.6M	11.01%	32.95%	9.9M
DSGC (ours)	<b>18.72%</b>	<b>44.33%</b>	5.7M	<b>7.31%</b>	<b>27.29%</b>	9.9M
CNN (VGG-13) (Simonyan and Zisserman, 2014)	18.03%	43.42%	18M	6.86%	26.86%	18M
CNN (Xception) (Chollet, 2016)	17.07%	41.54%	3.1M	7.08%	26.84%	3.1M

Table 1: Test-set error rates on CIFAR10 and CIFAR100. DSGC has the best performance among the graph-based convolution method group (first six methods), and is comparable to the state-of-the-art grid-based convolution methods (VGG-13 and Xception) which are tailed for image classification.

### 5.3 Evaluation on Time Series Forecasting

In time-series forecasting, we are usually interested in how to effectively utilize the geometric information about sensor networks. For example, how to incorporate the longitudes/latitudes of sensors w.r.t. temporal cloud movement is a challenge in spatiotemporal modeling for predicting the energy output of solar energy farms in the United States. Appendix B.2 provides the formal definition of this task.

We choose three publicly available benchmark datasets for this task:

- The U.S Historical Climatology Network (USHCN)<sup>3</sup> dataset, used in Bahadori et al. (2014), contains daily climatological data from 1,218 meteorology sensors over the years from 1915 to 2000. The sequence length is 32,507. It includes five subsets, and each has a

<sup>3</sup>[http://cdiac.ornl.gov/epubs/ndp/ushcn/daily\\_doc.html](http://cdiac.ornl.gov/epubs/ndp/ushcn/daily_doc.html)

climate variable: (1) maximum temperature, (2) minimum temperature, (3) precipitation, (4) snowfall and (5) snow depth. We use daily maximum temperature data and precipitation data, and refer them as the **TMAX** and **PRCP** sets, respectively.

- The solar power production records in the year of 2006 has the data with the production rate of every 10 minutes from 1,082 solar power stations in the west of the U.S. The sequence length is 52,560. We refer this set of data as **Solar**.

All the datasets have been split into the training set (60%), the validation set (20%) and the test set (20%) in chronological order.

Table 2 summarizes the evaluation results of all the methods, where the performance is measured using the Root Square Mean Error (RMSE). The best result on each dataset is highlighted in boldface. Overall, our proposed method (DSGC) has the best performance on all the datasets, demonstrating its strength in capturing informative local propagation patterns both temporally and spatially. In Appendix B.2, we include more comparisons with the pure temporal methods.

Method	TMAX	PRCP	Solar
DCNN	6.5188	29.0424	0.02652
ChebyNet	5.5823	27.1298	0.02531
GCN	5.4671	27.1172	0.02512
MoNet (with GAT)	5.8263	26.8076	0.02564
MPNN	5.3331	26.4766	0.02496
DSGC (ours)	<b>5.1438</b> ( $\pm 0.0498$ )	<b>25.8228</b> ( $\pm 0.249$ )	<b>0.02453</b> ( $\pm 0.00022$ )

Table 2: Test-set performance for graph convolution methods on time series prediction tasks measuring in RMSE. For our method, we report the standard deviation of the performance by running the model with 10 random seeds.

#### 5.4 Evaluation on Document Categorization

Following the experiment in Defferrard et al. (2016), we test DSGC and other baselines in the text categorization application, and use the 20NEWS dataset (Joachims (1996)) for our experiments. 20NEWS consists of 18,845 text documents with 20 topic labels. Individual words in the document vocabulary are the nodes in the graph for convolution. Each node has its word embedding vector generated by Word2Vec algorithm (Mikolov et al. (2013)) on the same corpus. Following the experiment settings in Defferrard et al. (2016) we select the top 1000 most frequent words as the nodes. Table 3 summarizes the results of the graph convolution methods plus three popular traditional classifiers (Linear SVM, Multivariate Naive Bayes and Softmax). DSGC has the best result on this dataset. Notice that the traditional classifiers are trained and tested with the feature set of the top 1000 words, which is the same setting as in the graph convolution models. If all words are used, traditional classifiers would have higher performance.

Method	Accuracy
Linear SVM <sup>†</sup>	65.90%
Multinomial NB <sup>†</sup>	68.51%
Softmax <sup>†</sup>	66.28%
FC2500 <sup>†</sup>	64.64%
FC2500-FC500 <sup>†</sup>	65.76%
DCNN	70.35%
ChebyNet	70.92%
GCN	71.01%
MoNet (with GAT)	70.60%
MPNN	71.58%
DSGC (ours)	<b>72.11%</b> ( $\pm 0.285$ )

Table 3: Accuracy on the validation set of 20NEWS. Results marked with <sup>†</sup> come from Defferrard et al. (2016). The number in the parenthesis is the standard deviation.

## 6 Conclusion

This paper presents a unified view of graph convolution and grid-based convolution methods, and proposes the novel DSGC approach that is applicable to non-grid spatial data. DSGC subsumes several existing graph convolution methods as special cases and is compatible to depthwise separable convolution for image classification by performing channel-special filters learning in data manifold. The proposed DSGC yields state-of-the-art performance on multi-domain benchmark datasets with a relatively small number of model parameters, reasonable computation cost, and is easy to be plugged in different neural network architectures. For future research we plan to extend DSGC to a broader

range of problems, including social network and citation graph analysis, where the spatial coordinates of the nodes (node embeddings) can be jointly learned along with the convolution filters, or defined by node embedding algorithm.

## References

- Atwood, J. and Towsley, D. (2016). Diffusion-convolutional neural networks. In *Advances in Neural Information Processing Systems*, pages 1993–2001.
- Bahadori, M. T., Yu, Q. R., and Liu, Y. (2014). Fast multivariate spatio-temporal analysis via low rank tensor learning. In *Advances in neural information processing systems*, pages 3491–3499.
- Boscaini, D., Masci, J., Rodolà, E., and Bronstein, M. (2016). Learning shape correspondence with anisotropic convolutional neural networks. In *Advances in Neural Information Processing Systems*, pages 3189–3197.
- Bronstein, M. M., Bruna, J., LeCun, Y., Szlam, A., and Vandergheynst, P. (2017). Geometric deep learning: going beyond euclidean data. *IEEE Signal Processing Magazine*, 34(4):18–42.
- Bruna, J., Zaremba, W., Szlam, A., and LeCun, Y. (2013). Spectral networks and locally connected networks on graphs. *arXiv preprint arXiv:1312.6203*.
- Chollet, F. (2016). Xception: Deep learning with depthwise separable convolutions. *arXiv preprint arXiv:1610.02357*.
- Defferrard, M., Bresson, X., and Vandergheynst, P. (2016). Convolutional neural networks on graphs with fast localized spectral filtering. In *Advances in Neural Information Processing Systems*, pages 3844–3852.
- Gilmer, J., Schoenholz, S. S., Riley, P. F., Vinyals, O., and Dahl, G. E. (2017). Neural message passing for quantum chemistry. *arXiv preprint arXiv:1704.01212*.
- Howard, A. G., Zhu, M., Chen, B., Kalenichenko, D., Wang, W., Weyand, T., Andreetto, M., and Adam, H. (2017). Mobilenets: Efficient convolutional neural networks for mobile vision applications. *arXiv preprint arXiv:1704.04861*.
- Hu, J., Shen, L., and Sun, G. (2017). Squeeze-and-excitation networks. *arXiv preprint arXiv:1709.01507*.
- Huang, G., Liu, Z., Weinberger, K. Q., and van der Maaten, L. (2016). Densely connected convolutional networks. *arXiv preprint arXiv:1608.06993*.
- Joachims, T. (1996). A probabilistic analysis of the rocchio algorithm with tfidf for text categorization. Technical report, Carnegie-mellon univ pittsburgh pa dept of computer science.
- Kingma, D. and Ba, J. (2014). Adam: A method for stochastic optimization. *arXiv preprint arXiv:1412.6980*.
- Kipf, T. N. and Welling, M. (2016). Semi-supervised classification with graph convolutional networks. *arXiv preprint arXiv:1609.02907*.
- Krizhevsky, A. and Hinton, G. (2009). Learning multiple layers of features from tiny images.
- Lai, G., Chang, W.-C., Yang, Y., and Liu, H. (2017). Modeling long-and short-term temporal patterns with deep neural networks. *arXiv preprint arXiv:1703.07015*.
- LeCun, Y., Bengio, Y., et al. (1995). Convolutional networks for images, speech, and time series. *The handbook of brain theory and neural networks*, 3361(10):1995.
- LeCun, Y., Bengio, Y., and Hinton, G. (2015). Deep learning. *Nature*, 521(7553):436–444.
- Li, Y., Yu, R., Shahabi, C., and Liu, Y. (2017). Graph convolutional recurrent neural network: Data-driven traffic forecasting. *arXiv preprint arXiv:1707.01926*.

- Masci, J., Boscaini, D., Bronstein, M., and Vandergheynst, P. (2015). Geodesic convolutional neural networks on riemannian manifolds. In *Proceedings of the IEEE international conference on computer vision workshops*, pages 37–45.
- Mikolov, T., Sutskever, I., Chen, K., Corrado, G. S., and Dean, J. (2013). Distributed representations of words and phrases and their compositionality. In *Advances in neural information processing systems*, pages 3111–3119.
- Monti, F., Boscaini, D., Masci, J., Rodolà, E., Svoboda, J., and Bronstein, M. M. (2016). Geometric deep learning on graphs and manifolds using mixture model cnns. *arXiv preprint arXiv:1611.08402*.
- Schütt, K., Kindermans, P.-J., Felix, H. E. S., Chmiela, S., Tkatchenko, A., and Müller, K.-R. (2017). SchNet: A continuous-filter convolutional neural network for modeling quantum interactions. In *Advances in Neural Information Processing Systems*, pages 992–1002.
- Shuman, D. I., Narang, S. K., Frossard, P., Ortega, A., and Vandergheynst, P. (2013). The emerging field of signal processing on graphs: Extending high-dimensional data analysis to networks and other irregular domains. *IEEE Signal Processing Magazine*, 30(3):83–98.
- Simonyan, K. and Zisserman, A. (2014). Very deep convolutional networks for large-scale image recognition. *arXiv preprint arXiv:1409.1556*.
- Szegedy, C., Vanhoucke, V., Ioffe, S., Shlens, J., and Wojna, Z. (2016). Rethinking the inception architecture for computer vision. In *Proceedings of the IEEE Conference on Computer Vision and Pattern Recognition*, pages 2818–2826.
- Veličković, P., Cucurull, G., Casanova, A., Romero, A., Liò, P., and Bengio, Y. (2017). Graph attention networks. *arXiv preprint arXiv:1710.10903*.
- Xingjian, S., Chen, Z., Wang, H., Yeung, D.-Y., Wong, W.-K., and Woo, W.-c. (2015). Convolutional lstm network: A machine learning approach for precipitation nowcasting. In *Advances in neural information processing systems*, pages 802–810.
- Zhu, X., Ghahramani, Z., and Lafferty, J. D. (2003). Semi-supervised learning using gaussian fields and harmonic functions. In *Proceedings of the 20th International conference on Machine learning (ICML-03)*, pages 912–919.

## A Additional Experiment

### A.1 DSGC with Multiple Neural Architectures

As the proposed DSGC is mathematically compatible with the traditional convolution method by performing channel special filter learning within one-layer, naturally, we can directly replace the convolution layers of general deep convolution frameworks with the DSGC modules while keeping a similar performance without modifying the framework structure. We examine DSGC with the following frameworks which are popular in recent years for standard convolution over images: (1) Inception (Szegedy et al., 2016), (2) DenseNet framework (Huang et al., 2016) and (3) Squeeze-and-Excitation block (Hu et al., 2017). The details of those architectures are included in the Appendix B. The results are presented in Table 4. Clearly, combined with the advantageous architectures, the performance of DSGC in image classification can be further improved (DSGC-DenseNet over DSGC-VGG-13). It demonstrates that the DSGC can easily enjoy the benefits of framework design for free from the traditional 2d-convolution network community.

### A.2 Training Time Comparison

In Table 5, we report the mean training time per epoch for GCN, DSGC and MoNet. The proposed DSGC computes the convolution weight for each edge in the graph, which requires more computation resources compared to GCN. However, we always perform the graph convolution on a sparse k-nearest neighbor graph, where the number of edges grows only linearly with the node size. Therefore the training is fairly efficient. Notably, DSGC consistently performs better than all graph convolution methods with around 1.5x-4x running time compared to the fastest graph convolution framework

Method	Subsampled Images			Original Images		
	CIFAR10	CIFAR100	#params	CIFAR10	CIFAR100	#params
DSGC-VGG-13	18.72%	44.33%	5.7M	7.31%	27.29%	9.9M
DSGC-INCEPTION	18.27%	43.41%	9.9M	<b>6.44%</b>	28.55%	12M
DSGC-DenseNet	17.17%	43.34%	2.7M	7.14%	<b>26.50%</b>	2.9M
DSGC-SE	18.71%	44.15%	6.1M	7.00%	27.26%	10M
VGG-13	18.03%	43.42%	18M	6.86%	26.86%	18M
Xception	<b>17.07%</b>	<b>41.54%</b>	3.1M	7.08%	26.84%	3.1M

Table 4: Test-set error rates of DSGC-based architectures (first group) and CNNs (second group)

(GCN). And MoNet, which also learns multiple filters in a layer but without the channel separation technique applied for DSGC, would be 1x slower than the proposed DSGC method.

Method	CIFAR10	TMAX	20news
GCN	1.75	0.465	0.207
MoNet	6.87	2.81	0.550
DSGC (ours)	3.81	1.73	0.280

Table 5: Training time per epoch for GCN, MoNet and DSGC in three benchmark datasets, measured in minutes.

## B Experiment Detail

### B.1 Implementation Details of CIFAR Experiment

Layers	VGG13	DSGC-VGG13	DSGC-DenseNet
Convolution	$[3 \times 3 \text{ conv}] \times 2$	$[9\text{-conv}] \times 2$	$[9\text{-conv}] \times 6$
Transition			1-conv
Pooling	$2 \times 2$ max-pooling	4 max-pooling	
Convolution	$[3 \times 3 \text{ conv}] \times 2$	$[9\text{-conv}] \times 2$	$[9\text{-conv}] \times 12$
Transition			1-conv
Pooling	$2 \times 2$ max-pooling	4 max-pooling	
Convolution	$[3 \times 3 \text{ conv}] \times 2$	$[9\text{-conv}] \times 2$	$[9\text{-conv}] \times 24$
Transition			1-conv
Pooling	$2 \times 2$ max-pooling	4 max-pooling	
Convolution	$[3 \times 3 \text{ conv}] \times 2$	$[9\text{-conv}] \times 2$	$[9\text{-conv}] \times 16$
Transition			1-conv
Pooling	$2 \times 2$ max-pooling	4 max-pooling	
Convolution	$[3 \times 3 \text{ conv}] \times 2$	$[9\text{-conv}] \times 2$	
Pooling	$2 \times 2$ max-pooling	4 max-pooling	
Classifier	512D fully-connected, softmax		

Table 6: Neural Network architecture for CIFAR datasets. Please see the text for more details.

In section 5.2 and A.1, we conduct the experiment on the CIFAR10 and CIFAR100 datasets. We will introduce the architecture settings for the DSGC and baseline models. Table 6 illustrates the basic architecture used in the experiment. In the DSGC-VGG13 and DSGC-DenseNet models, the  $k$ -conv refers to the spatial convolution (Eq.5) with  $k$ -nearest neighbors as the neighbor setting. So the 1-conv is the same as the  $1 \times 1$  conv, which is doing linear transformation on channels. The hidden dimensions of VGG13 and DSGC-VGG13 are set as  $\{256, 512, 512, 512\}$  and  $\{256, 512, 512, 1024\}$ . The growth rate of DSGC-DenseNet is 32. And the baseline graph and geometric convolution methods use the identical architecture as DSGC-VGG13. For the subsampled CIFAR experiment, We eliminate the first convolution, transition and pooling layer, and change the spatial convolution from 9-conv to  $\{16\text{-conv}, 12\text{-conv}, 8\text{-conv}, 4\text{-conv}\}$ . For the DSGC-SE, we follow the method described in Hu et al. (2017) to add the SE block to DSGC-VGG13 architecture. We use the dropout scheme described in Huang et al. (2016) for the DSGC-DenseNet model, and add the dropout layer after the pooling layer

for VGG13 and DSGC-VGG13 models. For the DSGC-Inception model, we imitate the design of the Inception Network (Szegedy et al. (2016)). The key idea is letting a convolution layer have different size of convolution filters. We use a simple example as our Inception module, which is illustrated in Figure 2.

For the CNN model, we still format the input signal in the matrix shape. The signals in invalid points are set as 0. Furthermore, to perform the fair comparison with standard CNN in the subsampled situation, we append a mask matrix as an additional channel for input signals to indicate whether the pixel is valid or not. For the ChebyNet, we set the polynomial order as  $K = 3$ .

The pooling layer is implemented by K-means clustering. The centroid of each clusters is regarded as the new node after pooling, and its hidden vector is the mean or max over the nodes in that cluster. Notice that, we only normalize the input signals to  $[0,1]$  and do not adopt any other data preprocessing or augmentation tricks.

For the  $\Delta_{ij}$  used in DSGC and MoNet, we use a 5 dimension feature vector. We denote the coordinate of  $i$ -th node as  $(x_i, y_i)$ , and  $\Delta x_{ij} = x_i - x_j, \Delta y_{ij} = y_i - y_j, \Delta d_{ij} = \Delta x_{ij}^2 + \Delta y_{ij}^2$ . Then  $\Delta_{ij} = (\text{sign}(\Delta x_{ij}), |\Delta x_{ij}|, \text{sign}(\Delta y_{ij}), |\Delta y_{ij}|, \Delta d_{ij})$ .

The same learning schedule is applied to all models. We use SGD to train the model for 400 epochs. The initial learning rate is 0.1, and is divided by 10 at 50% and 75% of the total number of training epochs.

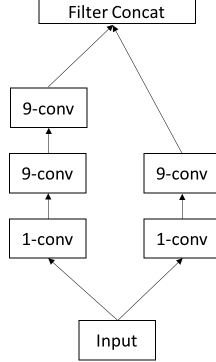


Figure 2: Inception Module

## B.2 Implementation Details of Time Series Prediction

Firstly, we will give the formal definition of the time series forecasting, that is, spatiotemporal regression problem. We formulate the the spatiotemporal regression problem as a multivariate time series forecasting task with the sensors' location as the input. More formally, given a series of time series signals observed from sensors  $\mathbf{Y} = \{\mathbf{y}_1, \mathbf{y}_2, \dots, \mathbf{y}_T\}$  where  $\mathbf{y}_t \in \mathbb{R}^n$  and  $n$  are the number of sensors, and the locations of sensors  $\mathbf{L} = \{\mathbf{l}_1, \mathbf{l}_2, \dots, \mathbf{l}_n\}$  where  $\mathbf{l}_i \in \mathbb{R}^2$  and indicates the coordinate of the sensor, the task is to predict a series of future signals in a rolling forecasting fashion. That being said, to predict  $\mathbf{y}_{T+h}$  where  $h$  is the desirable horizon ahead of the current time stamp  $T$ , we assume  $\{\mathbf{y}_1, \mathbf{y}_2, \dots, \mathbf{y}_T\}$  are available. Likewise, to predict the signal of the next time stamp  $\mathbf{y}_{T+h+1}$ , we assume  $\{\mathbf{y}_1, \mathbf{y}_2, \dots, \mathbf{y}_T, \mathbf{y}_{T+1}\}$  are available. In this paper, we follow the setting of the autoregressive model. Define a window size  $p$  which is a hyper-parameter firstly. The model input at time stamp  $T$  is  $\mathbf{X}_T = \{\mathbf{y}_{T-p+1}, \dots, \mathbf{y}_T\} \in \mathbb{R}^{n \times p}$ . In the experiments of this paper, the horizon is always set as 1.

Intuitively, different sensors may have node-level hidden features influencing its propagation patterns and final outputs. For each node, we let the model learn a node embedding vector and concatenate it with the input signals. The embedding size is tuned according to the validation set. By using this trick, each node has limited freedom to interface with its propagation patterns.

One thing readers may notice is that there are 10% data in USHCN dataset missing. To deal with that, we add an additional feature channel to indicate which point is missing. For the time series models, we tune the historical window  $p$  according to the validation set. For the rest of models, we set the

window size  $p = 18$  for Solar dataset and  $p = 6$  for USHCN datasets. The network architecture used in this task is 7 convolution layers followed by a regression layer. The  $\Delta_{ij}$  setting is the same as the previous one. We use the Adam optimizer (Kingma and Ba, 2014) for this task, and train each model 200 epochs with learning rate 0.001.

Except for the graph convolution methods, we also add in traditional methods of time series forecasting for comparison, such as (1) Autoregressive model (AR) which predicts future signal using a window of historical data based on a linear assumption about temporal dependencies, (2) Vector autoregressive model (VAR) which extends AR to the multivariate version, namely, the input is the signals from all sensors in the history window, and (3) the LSTNet deep neural network model (Lai et al., 2017) which combines the strengths of CNN, RNN and AR. None of those methods is capable of leveraging locational dependencies via graph convolution.

Method	TMAX	PRCP	Solar
AR	8.2354	30.3825	0.03195
VAR	17.9743	29.2597	0.03296
LSTNet	10.1973	29.0624	0.02865
DCNN	6.5188	29.0424	0.02652
ChebyNet	5.5823	27.1298	0.02531
GCN	5.4671	27.1172	0.02512
MoNet (with GAT)	5.8263	26.8076	0.02564
MPNN	5.3331	26.4766	0.02496
DSGC (ours)	<b>5.1438</b> ( $\pm 0.0498$ )	<b>25.8228</b> ( $\pm 0.249$ )	<b>0.02453</b> ( $\pm 0.00022$ )

Table 7: Test-set performance for graph convolution methods on time series prediction tasks measuring in RMSE. For our method, we report the standard deviation of the performance by running the model with 10 random seeds.

Table 2 summarizes the evaluation results of all the methods, where the performance is measured using the Root Square Mean Error (RMSE). The best result on each dataset is highlighted in boldface. The group of the first three methods does not leverage the spatial or locational information in data. The second group (graph-based convolution methods) consists of the neural network models which leverage the spatial information about sensor networks. The methods in the second group clearly outperform the methods in the first one, which does not explicitly model the spacial correlation within sensor networks.

### B.3 Implementation Details of Document Categorization

The data preprocessing follows the experiment details in Defferrard et al. (2016). And the network architecture for all models is 5 convolution layers followed by two MLP layers as the classifier. After each convolution layer, a dropout layer is performed with dropout rate of 0.5. The nodes' coordinate is the word embedding, and the method to calculate  $\Delta_{ij}$  is similar to the previous ones. The optimizer used in this task is the same as the CIFAR experiment.